fire

MDPI

Article

Numerical Modeling of Hydrogen Combustion: Approaches and Benchmarks

Ivan Yakovenko * and Alexey Kiverin

Joint Institute for High Temperatures of the Russian Academy of Sciences, Izhorskaya St. 13 Bd.2, Moscow 125412, Russia; alexeykiverin@gmail.com
* Correspondence: yakovenko.ivan@bk.ru

Abstract: The paper is devoted to the analysis of two different approaches for the numerical simulation of gaseous combustion. The first one is based on a full system of Navier-Stokes equations describing the dynamics of the compressible reactive medium, while the second one utilizes low-Mach number approximation. The compressible model is realized by the traditional low-order numerical scheme and the contemporary CABARET method. The low-Mach approach is implemented on the base of a widely known FDS numerical scheme. The benefits and disadvantages of compressible and low-Mach approaches are discussed and demonstrated on a specially developed set of problem setups, applicable for validation and verification of the numerical methods for combustion analysis. In particular, the laminar flame velocity test, spherical bomb test, and multidimensional modeling of combustion development inside the rectangular closed vessel are performed via both techniques that allowed to determine the applicability limits of the low-Mach number approximation.

Keywords: numerical modeling; gaseous combustion; compressibility effects; low-Mach approximation; validation and verification

check for updates

Citation: Yakovenko, I.; Kiverin, A. Numerical Modeling of Hydrogen Combustion: Approaches and Benchmarks. *Fire* **2023**, *6*, 239. https://doi.org/10.3390/fire6060239

Academic Editor: Ali Cemal Benim

Received: 22 May 2023
Revised: 12 June 2023
Accepted: 13 June 2023
Published: 16 June 2023

1. Introduction

Today numerical modeling became a powerful tool for complex combustion process analysis. Together with the experimental observations, computational techniques allow comprehensive investigation of various combustion modes, which can develop in volumes filled with reactive gaseous mixtures. Numerical modeling is particularly important for studying high-speed processes, such as flame acceleration and deflagration-to-detonation transition in gaseous mixtures [1,2], in complex fuels [3], and the propagation of detonation waves [4]. Determination of the mechanisms responsible for various combustion modes formation and transitions between them and prediction of the damages related to the dynamic and thermal loads associated with the combustion development is crucial for reliable combustion and explosion safety systems design and risk mitigation measures.

Despite the sufficient progress in techniques and resources available for computations, reliable combustion modeling is still a challenging problem. Tight coupling between gas-dynamic flows, chemical kinetics, and molecular transfer makes it very demanding to perform detailed numerical modeling on spatial and temporal scales characteristic for real-world applications, especially for analyzing large-scale fires or combustion within propulsion and energy devices. Model simplifications commonly used to cut computational costs include reduced or lumped chemical kinetic schemes, sub-grid turbulence models, and various approximations of the flow features. Among the latter, the low-Mach approximation is one of the most used. It allows softening restrictions on the time step related to the necessity to reproduce individual acoustic perturbations propagating with the speed of sound. Instead, the average acoustic field is calculated as a continuous distribution of the pressure perturbation. As a result, the calculation time step can be sufficiently increased, and calculations may be performed on greater spatial and temporal scales than with techniques developed for a Navier-Stokes equations system describing dynamics of

compressible medium. For today low-Mach model is extensively used for the computations of flame instability development [5,6], turbulent mixing inside a cylinder of the internal combustion engine [7], jet flames [8] and other problems. However, such an approximation has only a limited range of possible applications. High-speed reactive flow development, associated with the formation of intense shock waves and complex acoustic fields, cannot be reliably reproduced with a low-Mach approach. For these problems, it is required to fully resolve compressibility effects, such as the generation and propagation of compression and shock waves and interactions between waves, flame, and acoustic fields.

Among various computational techniques realizing low-Mach number approximation, the approach implemented in Fire Dynamics Simulator (FDS) computational package [9] proves itself very useful for modeling large-scale compartment fires [10,11]. Originally it utilized lumped species chemical kinetic scheme, LES subgrid model of turbulent combustion, and constant heat capacity of the mixture. The FDS approach was not widely utilized for comprehensive numerical simulations of combustion using detailed chemical kinetic schemes, and precise molecular transport models and real equations of state. For the first time, such calculations via FDS approach were recently performed for the analysis of the buoyancy-driven combustion in premixed ultra-lean hydrogen-air mixtures [12] and allowed determining mechanisms of the flame extinguishing due to convective flows. Here the implementation of the FDS approach for solving conservation laws on the basis of the in-house computational software NRG [13] is employed to evaluate further the capabilities of low-Mach number approximation and the FDS numerical algorithm for detailed combustion modeling. NRG package contains models for heat transfer, viscosity, multicomponent diffusion, and capability for using detailed chemical kinetic schemes. Together with the FDS approach for solving gas dynamic governing equations in low-Mach approximation, the NRG package contains the traditional low-order finite-difference method "coarse" particles method (CPM) [14] and the contemporary computational technique CABARET for solving the Navier-Stokes equation system for the compressible gaseous mixture [15,16]. CPM is a robust computational approach that allows for solving a wide range of combustion problems. However, the main drawback of this technique is a relatively high numerical dissipation. On the one side, high dissipation makes it very versatile and applicable to studying general features of different modes of gas-dynamic flows, but on the other side small-scale flow features, such as acoustic and vortical perturbations, cannot be reliably reproduced. In turn, CABARET has several distinct features making this numerical scheme highly suitable for modeling complex flows in reactive gaseous mixtures. Among the most important advantages are the compact computational stencil, convenient for high-performance computations, low dissipation and dispersion errors, and the absence of artificial flux limiting procedures.

An acute problem in the field of computational analysis of combustion is related to the reproducibility of the obtained results and methods for the evaluation of numerical schemes in terms of applicability for the reliable modeling of complex transient reactive flows. Although there is a vast amount of test problems in conventional computational fluid dynamics, there is still a lack of generally accepted approaches for validation and verification of the numerical techniques used for combustion modeling [17]. Combustion is accompanied by a large number of processes, such as molecular transport, chemical kinetics, and gas dynamics. The correctness of the reproduction of those processes can be estimated separately, but it does not guarantee the overall accuracy of the reactive flow modeling. There are attempts to establish validation and verification routines for particular combustion problems, such as gas turbine combustors modeling [18], simulation of jet flames [19], and premixed turbulent flames [20]. An overview of experimental data that can be used for validation purposes can be found in [21,22]. However, most of the experimental data and proposed validation and verification approaches are developed for complex combustion processes and particular applications. Such problems require implementing approximate subgrid turbulence models and simplified chemical kinetic schemes. Thereby correct identification of the source of discrepancies is a complicated

problem, not to mention determining their reasons. For engineering purposes, such an approach is justified, but in academic research more rigorous and controlled routines for validation and verification are required. This paper is devoted to the evaluation of the ability for combustion modeling by three numerical approaches, FDS, CPM, and CABARET, based on the proposed set of test problems with a step-by-step increase in complexity of the flow, starting from steady one-dimensional combustion and ending at non-steady multidimensional flame development. The testing methodology follows that proposed in [17] and is intended to assess possible limitations of the computational techniques and underlying physical models of hydrogen combustion.

2. Mathematical Model

A full set of Navier-Stokes equations of the multicomponent reactive hydrogen-air mixture taking into account compressibility, viscosity, heat transfer, multicomponent diffusion, real equation of state, and detailed scheme of chemical kinetics scheme [23] is solved via a contemporary CABARET numerical scheme and traditional approach CPM. Governing equations are given below:

$$\frac{\partial \rho}{\partial t} + \frac{\partial(\rho u_i)}{\partial x_i} = 0 \tag{1}$$

$$\frac{\partial(\rho Y_k)}{\partial t} + \frac{\partial(\rho u_i Y_k)}{\partial x_i} = \frac{\partial\left(\rho Y_k V_{k,j}\right)}{\partial x_i} + \rho\dot{\omega}_k \tag{2}$$

$$\frac{\partial(\rho u_j)}{\partial t} + \frac{\partial(\rho u_i u_j)}{\partial x_i} = \left[\frac{\partial}{\partial x_i}\left(\sigma_{ji} - \delta_{ij} p\right)\right] \tag{3}$$

$$\begin{aligned}\frac{\partial(\rho E)}{\partial t} + \frac{\partial(\rho u_i E)}{\partial x_i} &= \left[\frac{\partial}{\partial x_i}\left(u_j\sigma_{ji} - u_i p\right)\right] + \\ &+ \left[\frac{\partial}{\partial x_i}\left(\kappa(T)\frac{\partial T}{\partial x_i}\right) + \rho\sum_k \frac{h_k}{m_k}\left(\frac{\partial Y_k}{\partial t}\right)\right]\end{aligned} \tag{4}$$

$$\sigma_{ij} = \mu(T)\left(\frac{\partial u_i}{\partial x_j} + \frac{\partial u_j}{\partial x_i} - \frac{2}{3}\delta_{ij}\frac{\partial u_m}{\partial x_m}\right) \tag{5}$$

where x_i—spatial coordinates, t—time, ρ—density, $Y_k = \rho_k/\rho$—k-th species mass fraction, p—pressure, T—temperature, u_i—mass velocity vector, $V_{k,i}$—k-th species diffusion velocity vector, $E = \varepsilon + \frac{1}{2}\left(\sum_i {u_i}^2\right)$—specific total energy, ε—specific inner energy, $\dot{\omega}_k$—chemical source term, $\kappa(T)$—thermal conductivity, $D_k(T)$—diffusion coefficient of k-th species, $\mu(T)$—viscosity coefficient, h_k—enthalpy of formation of k-th species, m_k—k-th specie molar mass, σ_{ij}—shear stress tensor components, δ_{ij}—Kronecker delta.

Mixture averaged transport coefficients such as viscosity $\mu(T)$, thermal conductivity $\kappa(T)$ and diffusion $D_k(T)$ are calculated from the first principles of the molecular kinetic theory. Mixture averaged viscosity coefficient $\mu(T)$ is obtained as:

$$\mu(T) = \frac{1}{2}\left[\sum_k X_k\mu_k + \left(\sum_k \frac{X_k}{\mu_k}\right)^{-1}\right] \tag{6}$$

where X_k—molar fraction of k-th species and viscosity coefficient of k-th species μ_k is calculated as follows [24]:

$$\mu_k(T) = \frac{5}{16}\frac{\sqrt{\pi M_k k_B T}}{\pi\sigma_k^2\Omega^{(2,2)}} \tag{7}$$

where $\Omega^{(2,2)}$—reduced collision integral depending on reduced temperature $T^* = k_B T/\varepsilon_k$ [25], σ_k—collision diameter, M_k—k-th atomic (molecular) mass, ε_k—Lennard-Jones potential well depth, k_B—Boltzmann constant. Values of σ_k, ε_k were taken from transport table accompanying chemical mechanism from [26].

Mixture averaged thermal conductivity:

$$\kappa(T) = \frac{1}{2}\left[\sum_k X_k \kappa_k + \left(\sum_k \frac{X_k}{\kappa_k}\right)^{-1}\right] \tag{8}$$

while thermal conductivity κ_k for each species [24]:

$$\kappa_k(T) = \frac{25}{32}\frac{\sqrt{\pi M_k k_B T}}{\pi \sigma_k^2 \Omega^{(2,2)}}\frac{c_{V_k}}{M_k}. \tag{9}$$

Diffusion velocities were calculated via zeroth-order approximation [27]:

$$V_{k,i}^* = \left(\frac{D_k(T)}{Y_k}\frac{\partial Y_k}{\partial x_i}\right) \tag{10}$$

where mass-averaged diffusion coefficient of k-th species D_k is obtained as [28]:

$$\frac{1}{D_k} = \sum_{j\neq k}^{N}\frac{X_j}{D_{kj}} + \frac{X_k}{1-Y_k}\sum_{j\neq k}^{N}\frac{Y_j}{D_{kj}} \tag{11}$$

where X_k—molar fraction of k-th component, D_{kj}—binary diffusion coefficient of a compound k into a compound j. Binary diffusion coefficients are calculated as follows [27,28]:

$$D_{kj} = \frac{3}{16}\frac{\sqrt{2\pi k_B^3 T^3/m_{kj}}}{p\pi\sigma_{kj}^2\Omega^{(1,1)}} \tag{12}$$

Diffusion velocity is corrected to satisfy $\sum_N Y_k V_{k,i} = 0$ [23,29] and is given by:

$$Y_k V_{k,i} = Y_k\left(V_{k,i}^* - V_{c,i}\right) = \left(D_k(T)\frac{\partial Y_k}{\partial x_i}\right) - Y_k\sum_N\left(D_k(T)\frac{\partial Y_k}{\partial x_i}\right) \tag{13}$$

Equations of state are based on temperature dependencies of specific enthalpies of k-th species h_k and specific constant volume heat capacities of k-th species c_{V_k}, expressed in NASA polynomial form with coefficients taken from [26].

$$p = \rho RT/\overline{M} \tag{14}$$

$$d\varepsilon = c_V(T)dT \tag{15}$$

where R—universal gas constant, $\overline{M}^{-1} = \sum_k Y_k/m_k$—the average molar mass, $c_V = \sum_k c_{V_k} Y_k$—specific constant volume heat capacity of the mixture, c_{V_k}—specific constant volume heat capacity of k-th species.

Balance-characteristic form of the CABARET algorithm [30] with second-order accuracy in space and time is utilized to solve the governing equations system (1)–(4). Traditional CPM approach [31] with first-order accuracy in space and second-order accuracy in time is implemented for comparison purposes and investigation of numerical viscosity effects. In both approaches, the time step is dynamically adjusted according to the Courant–Friedrichs–Lewy condition $CFL = \Delta t\left(\frac{\|\vec{u}\|+c}{\Delta x}\right) < 1$, where $c = \sqrt{\frac{p}{\rho}}$—velocity of sound.

The FDS approach utilizes low-Mach number approximation of the Navier-Stokes equations. According to this approximation, the total pressure p is decomposed into background pressure and perturbation [32]: $p(\vec{r},t) = \bar{p}(t) + \tilde{p}(\vec{r},t)$. The background pressure $\bar{p}(t)$ is calculated from the equation of state (14). Perturbation pressure $\tilde{p}(\vec{r},t)$ is obtained from the Poisson equation, derived from the momentum transport Equation (3):

$$\nabla^2 H = -\left[\frac{\partial}{\partial t}(\nabla \cdot \vec{u}) + \nabla \cdot \vec{F}\right] \tag{16}$$

where $H \equiv |\vec{u}|^2/2 + \tilde{p}/\rho$, $\vec{F} = -\vec{u} \times \vec{\omega} - \frac{1}{\rho}\left[\nabla \sigma_{ij}\right] - \tilde{p}\nabla\left(\frac{1}{\rho}\right)$, $\vec{\omega} = \nabla \times \vec{u}$—vorticity vector.

The Equation (16) is solved via V-cycle geometric multigrid approach [33]. The overall solution procedure follows the explicit second-order predictor/corrector scheme described in [9]. The time step is adjusted dynamically based on the Courant-Friedrichs-Lewy constraint $CFL = \Delta t\left(\frac{\|\vec{u}\|}{\Delta x} + |\nabla \cdot \vec{u}|\right) < 1$. TVD transport scheme with CHARM flux limiter [34] is used for scalar transport equations.

All three numerical techniques are realized on the base of the same in-house computational software NRG. Thereby all the molecular transport models and implementation of the chemical kinetics are preserved for considered numerical methods. A detailed chemical scheme consisting of 19 reactions between 8 chemically active components is used for the hydrogen oxidation process description [26].

3. Problem Setup

Three problem setups are considered. The first one is the laminar burning velocity test, namely the determination of the laminar burning velocity via one-dimensional calculations of the planar flame. Two different approaches are used. According to the first one, flame develops in a one-dimensional semi-closed channel and propagates toward the opened end after the ignition near the closed end of the channel. The solid wall boundary condition is implemented on the left end of the computational domain and the free outflow condition is set up on the right end of the computational domain. Here laminar burning velocity S_b can be obtained by tracking the flame velocity in the laboratory frame of reference $U_{f,L}$ and can be estimated as $S_b = U_{f,L}/\theta$, where expansion ratio $\theta = \rho_f/\rho_b$ is the ratio of densities of the fresh mixture ρ_f and burnt products ρ_b. The second approach for determining laminar burning velocity is also based on calculations in an opened channel. The inflow of the fresh mixture boundary condition is set on the left end of the computational domain, while the free outflow of combustion products is implemented on the right end of the computational domain. Here flame front is subjected to the counterflow of the fresh mixture, and via dynamic change of the fresh mixture flow velocity, one can obtain a flow velocity value corresponding to the flame stabilization, so the flame front becomes stationary. By definition, this flow velocity value coincides with the laminar burning velocity. This approach is used only with the FDS technique, as it occurs to be very sensitive towards acoustic perturbations, which impede flame stabilization.

The second problem is the flame development inside the spherical vessel of 20 cm diameter (1.3 L volume). Here calculations are performed in spherical symmetry. The left end of the computational domain is a symmetry point, and the solid wall condition is stated on the right end of the domain. This problem is intended to investigate combustion features under the influence of compression wave propagation at the background of the continuous pressure rise. In particular, it is of interest to define the limits of the low-Mach number approximation in the context of developed acoustic fields accompanying combustion.

The third problem is devoted to the analysis of the flame dynamics within the two-dimensional closed vessel and the influence of the compression waves on the flame front structure. Here the rectangular volume with dimensions 25 × 25 mm filled with hydrogen-air mixtures of various compositions is considered. All the boundaries represent solid walls. Flame is initiated in the middle of the volume and propagates outwardly.

4. Discussion

4.1. Laminar Burning Velocity Test

The results of the routine for determining the laminar burning velocity are presented in Figure 1a. Here meshes with different cell sizes are used to perform the convergence analysis. All considered techniques and methods for obtaining laminar burning velocity provide close results with mesh refining. Moreover, calculated values of the laminar burning velocity are within the scatter of the experimental data. It can be concluded that implemented techniques are capable of reproducing features of laminar combustion if the compression waves are not playing a crucial role in the flame dynamics. From the Figure 1a, it can be seen that the convergence rate is highest in the case of burning velocity estimation on the basis of flame dynamics in the opened channel. In semi-closed channels, convergence rates on the example of obtaining laminar burning velocity in stoichiometric mixture via CPM, FDS, and CABARET approaches are 1.2, 1.7, and 4.7, respectively. It can be concluded that a cell size of 100 μm provides a reliable estimation of the laminar burning velocity for the CABARET and FDS methods. In turn, the results obtained via the CPM method are generally overestimated and become close to experimental values only with the cell size of 50 μm. The small convergence rate and the necessity to utilize smaller cell sizes is a manifestation of the high numerical dissipation of the CPM technique compared to other considered methods. Based on that result, a cell size of 100 μm is employed in further calculations via CABARET and FDS, while for CPM computational cell with a cell size of 50 μm is used. Figure 1b provides the values of the expansion ratio obtained with different numerical schemes. The expansion ratio does not depend on the chosen approach for gas dynamics computations. That parameter depends solely on the thermodynamics and kinetics of combustion.

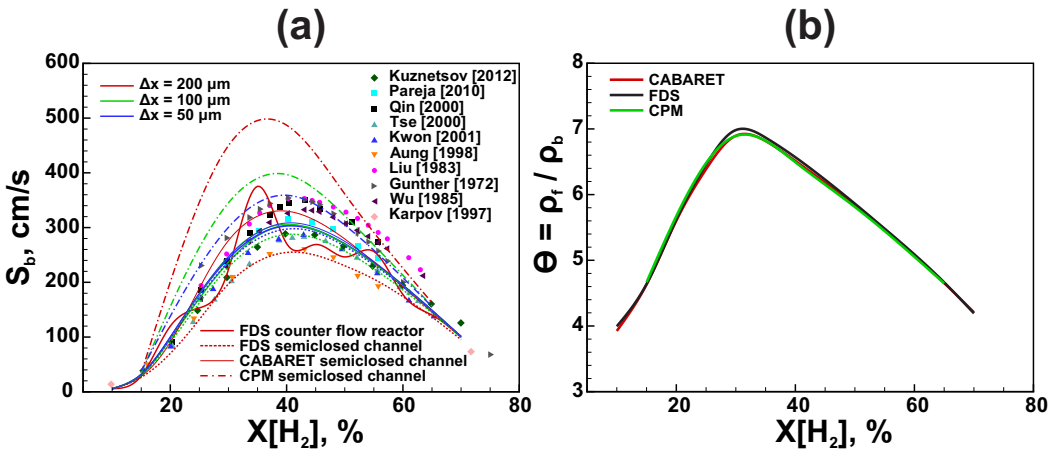

Figure 1. (**a**) Laminar burning velocity calculations via different approaches. Red lines—cell size 200 μm, green lines—cell size 100 μm, blue lines—cell size 50 μm. Signs—experimental values adopted from reviews by Sanchez and Williams [35] and Pareja et al. [36]; (**b**) expansion ratio θ calculated via FDS, CPM and CABARET techniques.

4.2. Spherical Vessel

Experimental facilities with a reaction chamber of spherical shape are commonly used for the analysis of the spherical freely propagating flame. Based on the obtained data, one can measure important characteristics of the flame evolution, such as combustion intensity, laminar burning velocity [37], cellular patterns due to instability development on the flame front [38], and many others. In Figure 2, time histories of the pressure inside the chamber calculated with FDS, CPM, and CABARET techniques for different mixture compositions are presented. It can be seen that low-Mach approximation causes an underestimation of the pressure rise increment in the considered mixtures. The results obtained via the FDS method are close to the compressible model only in the initial stages of combustion of lean compositions with moderate chemical reactivity. In the cases of higher chemical activity,

the compression waves play an important role in the flame dynamics already in the earlier stage of flame development and cause sufficient intensification of the combustion process. In turn, the overestimation of laminar burning velocity by the CPM technique leads to the overall increase in combustion process intensity compared to another compressible method CABARET. Figure 3 provides a clear visualization of how compression waves modify temperature and velocity profiles in the fresh mixture and combustion products. Here one can see that due to lower dissipation error, the compression waves pattern is more developed when using CABARET in comparison with the CPM result.

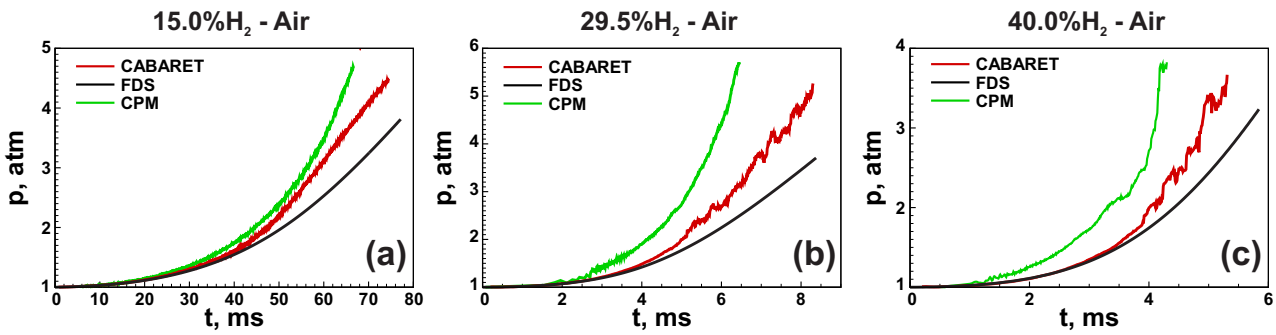

Figure 2. Pressure measurements on a wall of the spherical vessel. (**a**) 15.0% H_2-Air mixture, (**b**) 29.5% H_2-Air mixture, (**c**) 40.0% H_2-Air mixture. Solid black lines—FDS method, solid red lines—CABARET method (moving average), solid green lines—CPM method (moving average).

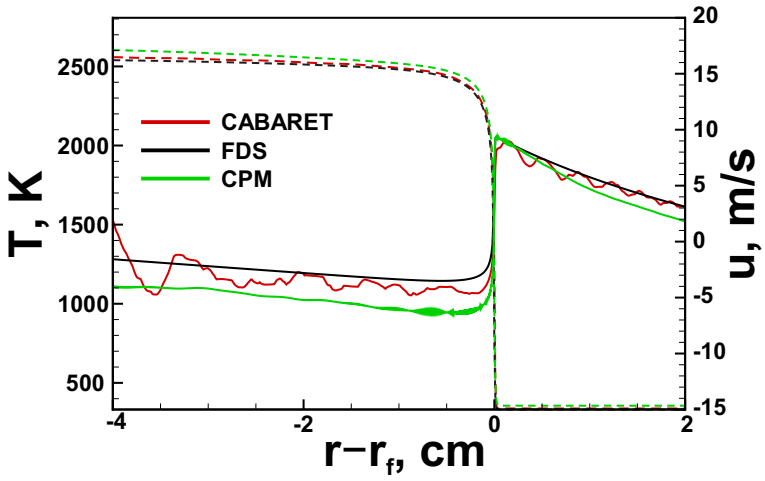

Figure 3. Temperature and velocity profiles in a spherical vessel filled with stoichiometric hydrogen-air mixture in a coordinate system related to the flame front location. Solid lines—velocity, dashed lines—temperature. Black lines—FDS method, red lines—CABARET method, green lines—CPM method. Time instant 4 ms.

4.3. Multidimensional Flame Development

Here we analyze flame evolution in a closed rectangular vessel obtained via CABARET, CPM, and FDS approaches. Compression waves emitted by the flame front during its evolution define the flow structure ahead of the flame. Peculiarities of the flow can have a crucial impact on the overall flame dynamics. Thus, in the case of combustion in the semi-opened channel, the development of the flow determines the flame acceleration in the initial stages of the combustion process [39]. In closed volume, the reflection of the compression waves from the reactor walls and its further interaction with the flame can sufficiently alter the topology of the flame, causing additional flame front corrugation [40]. In turn, the rise of the flame front surface due to the perturbation development increases combustion intensity. Thus, the correct reproduction of the acoustic patterns ahead of the flame is crucial for precise flame dynamics modeling. From the pressure curves depicted in Figure 4, one can

conclude that the correct reproduction of acoustic effects together with laminar burning velocity value has a substantial influence on the overall combustion dynamics. In Figure 5, flame front structures and vorticity distributions for the lean 15% hydrogen-air mixture (left column) in the cases of using FDS, CPM, and CABARET approaches are presented. It can be seen that the flame front obtained via the CABARET technique is more developed compared to the FDS and CPM results. Interaction between the compression waves ahead of the flame defines the formation of complex flow patterns containing small-scale vortical structures. These vortices interact with the flame, causing its local perturbation that leads to flame corrugation, intensification of the flame instability development, and increased intensity of the combustion process, which can be correctly modeled via the CABARET technique. In the case of the CPM method, the propagation of compression waves is also resolved within the model. However, the numerical dissipation leads to significant smearing of all flow perturbations. Thereby the effect of acoustic fields on the combustion dynamics is reduced. The FDS approach, on the contrary, cannot reproduce the acoustic pattern in the fresh mixture. Thus the flame front evolution here is governed solely by the intrinsic instability development. In the initial stage of the process, when the flame develops nearly as in an unconfined space, the leading role belongs to the laminar burning velocity value. Overestimation of this parameter leads to more intense combustion development at that stage in the case of the CPM approach compared to other methods (see Figure 4). Further, as the flame comes closer to the walls of the vessel, acoustic perturbations and instability development start to play a much more important role. Here only the CABARET approach can correctly predict the acoustic pattern and flame front corrugation, which make flame evolution more rapid. Despite higher combustion intensity, in the case of a stoichiometric H_2-Air mixture, this effect is less noticeable as the combustion is less prone to instability development. Here the leading role belongs to the correct reproduction of the laminar burning velocity parameter. A comparison of flame front structures and vorticity fields for a stoichiometric hydrogen-air mixture is presented in Figure 5 (right column).

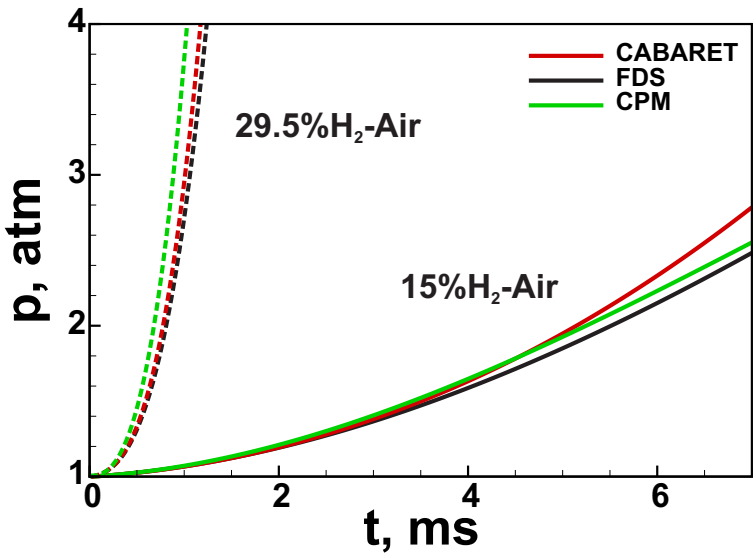

Figure 4. Pressure rise in a rectangular vessel filled with 15% hydrogen-air mixture (dashed lines) and 29.5% hydrogen-air mixture (solid lines) obtained via CABARET (moving average, red lines), FDS (black lines) and CPM (moving average, green lines) techniques.

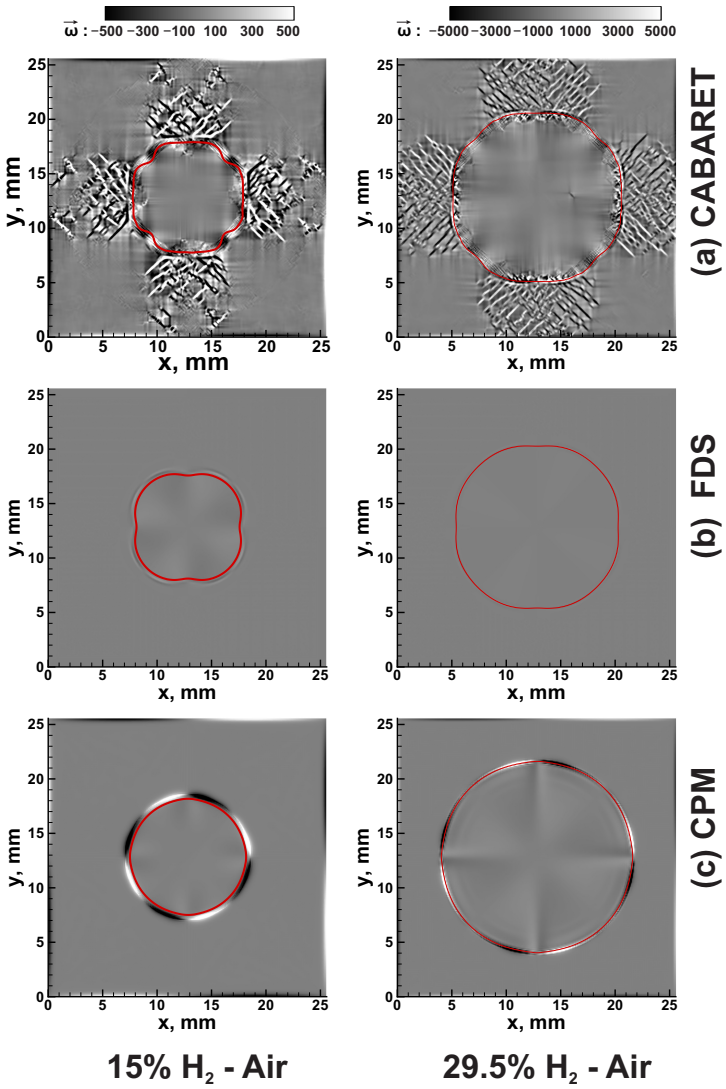

Figure 5. Vorticity field in a rectangular vessel filled with 15% hydrogen-air (left column, time instant 2100 ms) and stoichiometric hydrogen-air mixture (right column, time instant 610 ms) obtained via (**a**) CABARET technique (**b**) FDS technique (**c**) CPM technique. Red line represents temperature isoline T = 1500 K.

5. Conclusions

The paper presents the analysis of the capabilities of low-Mach number approximation implemented in the FDS approach in comparison with the compressible model realized by the CABARET and CPM numerical schemes.

- In opened systems, where the interaction between the compression waves and the flame front is not intense, the low-Mach approximation provides reliable solutions close to those obtained with the compressible model. Thus the difference in the estimation of laminar burning velocity via CABARET and FDS techniques is less than 6% for $\Delta x = 50$ µm.
- It is shown that the flame development within closed vessels, strongly affected by compression waves propagation, is not precisely reproduced within the framework of the low-Mach number approximation. The calculations in a spherical vessel show that the low-Mach model tends to underestimate the dynamics of pressure rise. The interaction between individual compression waves and the flame front causes its local acceleration or deceleration that leads to the overall greater intensity in the combustion process and faster pressure build-up.

- From the results of multidimensional calculations, it is shown that the combustion intensity is not the key factor defining the compression waves' impact. In mixtures susceptible to instability development, such as lean hydrogen-air mixtures, even low intense compression waves can trigger instability development and multidimensional evolution of the flame front, leading to a substantial change in the dynamics of the combustion process.
- On the example of the traditional CPM numerical method, it is shown that numerical dissipation errors act in a similar way to acoustic filtering in low Mach approximation, smearing acoustic perturbations and reducing their influence on the flame front structure evolution.

Author Contributions: Conceptualization, A.K. and I.Y.; methodology, I.Y.; software, I.Y.; validation, I.Y. and A.K.; formal analysis, I.Y.; investigation, I.Y.; resources, I.Y.; data curation, I.Y.; writing—original draft preparation, I.Y.; writing—review and editing, A.K.; visualization, I.Y.; supervision, A.K.; project administration, I.Y.; funding acquisition, I.Y. and A.K. All authors have read and agreed to the published version of the manuscript.

Funding: The work was financially supported by the state support of young Russian scientists grant MK-1784.2022.1.1.

Institutional Review Board Statement: Not applicable.

Informed Consent Statement: Not applicable.

Data Availability Statement: The datasets generated and/or analysed during the current study are available from the corresponding author on reasonable request.

Conflicts of Interest: The authors declare no conflict of interest.

Abbreviations

The following abbreviations are used in this manuscript:

FDS	Fire Dynamics Simulator
CABARET	Compact Accurately Boundary Adjusting-REsolution Technique
JANAF	Joint Army-Navy-Air Force
LES	Large Eddy Simulation
CPM	"Coarse" Particles Method
TVD	Total Variation Diminishing
CHARM	Cubic-parabolic High Accuracy Resolution Method

Nomenclature

R	universal gas constant
k_B	Boltzmann constant
x_i	spatial coordinates
t	time
ρ	density
Y_k	mass fraction of k-th species
X_k	molar fraction of k-th species
p	total pressure
T	temperature
E	specific total energy
c	velocity of sound
ε	specific inner energy
u_i	mass velocity vector
ω_i	vorticity vector
σ_{ij}	shear stress tensor components
$\kappa(T)$	thermal conductivity
$D_k(T)$	mass-averaged diffusion coefficient of k-th species
$\mu(T)$	viscosity coefficient

κ_k	thermal conductivity coefficient of k-th species
μ_k	viscosity coefficient of k-th species
D_{kj}	binary diffusion coefficient of a compound k into a compound j
$V_{k,i}$	k-th species diffusion velocity vector
m_k	k-th specie molar mass
M_k	atomic (molecular) mass of k-th species
$\overline{M}^{-1}$	mixture average molar mass
$\dot{\omega}_k$	chemical source term
h_k	enthalpy of formation of k-th species
$\Omega^{(2,2)}$	reduced collision integral
T^*	reduced temperature
σ_k	collision diameter of k-th species
ε_k	Lennard-Jones potential well depth
c_V	specific constant volume heat capacity of the mixture
c_{V_k}	specific constant volume heat capacity of k-th species
$\bar{p}$	background pressure
$\tilde{p}$	perturbation pressure
H	total pressure divided by the density (Bernoulli integral)
δ_{ij}	Kronecker delta

References

1. Houim, R.W.; Ozgen, A.; Oran, E.S. The role of spontaneous waves in the deflagration-to-detonation transition in submillimetre channels. *Combust. Theory Model.* **2016**, *20*, 1068–1087. [CrossRef]
2. Boeck, L.R.; Lapointe, S.; Melguizo-Gavilanes, J.; Ciccarelli, G. Flame propagation across an obstacle: OH-PLIF and 2-D simulations with detailed chemistry. *Proc. Combust. Inst.* **2017**, *36*, 2799–2806. [CrossRef]
3. Kiverin, A.; Yakovenko, I. Unsteady Combustion of the Heptane-in-Water Emulsion Foamed with Hydrogen–Oxygen Mixture. *Appl. Sci.* **2023**, *13*, 4829. [CrossRef]
4. Smirnov, N.N.; Nikitin, V.F.; Mikhal'chenko, E.V.; Stamov, L.I. Inhibition of Developed Detonation of a Hydrogen–Air Mixture by a Small Addition of a Hydrocarbon Inhibitor. *Combust. Explos. Shock Waves* **2022**, *58*, 564–570. [CrossRef]
5. Frouzakis, C.E.; Fogla, N.; Tomboulides, A.G.; Altantzis, C.; Matalon, M. Numerical study of unstable hydrogen/air flames: Shape and propagation speed. *Proc. Combust. Inst.* **2015**, *35*, 1087–1095. [CrossRef]
6. Berger, L.; Kleinheinz, K.; Attili, A.; Pitsch, H. Characteristic patterns of thermodiffusively unstable premixed lean hydrogen flames. *Proc. Combust. Inst.* **2019**, *37*, 1879–1886. [CrossRef]
7. Schmitt, M.; Frouzakis, C.E.; Tomboulides, A.G.; Wright, Y.M.; Boulouchos, K. Direct numerical simulation of the effect of compression on the flow, temperature and composition under engine-like conditions. *Proc. Combust. Inst.* **2015**, *35*, 3069–3077. [CrossRef]
8. Frouzakis, C.E.; Tomboulides, A.G.; Papas, P.; Fischer, P.F.; Rais, R.M.; Monkewitz, P.A.; Boulouchos, K. Three-dimensional numerical simulations of cellular jet diffusion flames. *Proc. Combust. Inst.* **2005**, *30*, 185–192. [CrossRef]
9. McGrattan, K.; McDermott, R.; Hostikka, S.; Floyd, J.; Vanella, M. Fire Dynamics Simulator Technical Reference Guide Volume 1: Mathematical Model. In *Technical Report NIST Special Publication 1018-1*; U.S. Department of Commerce, National Institute of Standards and Technology: Gaithersburg, MD, USA, 2019. [CrossRef]
10. Yang, W.; Abu Bakar, B.H.; Mamat, H.; Gong, L. A New, Green, Recyclable Fireproof Insulation Board for Use in Integrated Composite Structure Fire Protection Systems. *Fire* **2022**, *5*, 203. [CrossRef]
11. Gu, X.; Zhang, J.; Pan, Y.; Ni, Y.; Ma, C.; Zhou, W.; Wang, Y. Hazard analysis on tunnel hydrogen jet fire based on CFD simulation of temperature field and concentration field. *Saf. Sci.* **2020**, *122*, 104532. [CrossRef]
12. Yakovenko, I.; Kiverin, A.; Melnikova, K. Ultra-lean gaseous flames in terrestrial gravity conditions. *Fluids* **2021**, *6*, 21. [CrossRef]
13. Numerical Reactive Gas-Dynamics Package. Available online: https://github.com/yakovenko-ivan/NRG (accessed on 5 May 2023).
14. Grigoryev, Y.; Vshivkov, V.; Fedoruk, M. *Numerical "Particle-in-Cell" Methods Theory and Applications*; De Gruyter: Vienna, Austria, 2002.
15. Goloviznin, V.; Zaitsev, M.; Karabasov, S.; Korotkin, I. *New Computational Fluid Dynamics Algorithms for Multiprocessor Computers*; MSU Publishing: Moscow, Russia, 2013. (In Russian)
16. Karabasov, S.A.; Goloviznin, V.M. Compact Accurately Boundary-Adjusting high-REsolution Technique for fluid dynamics. *J. Comput. Phys.* **2009**, *228*, 7426–7451. [CrossRef]
17. Bykov, V.; Kiverin, A.; Koksharov, A.; Yakovenko, I. Analysis of transient combustion with the use of contemporary CFD techniques. *Comput. Fluids* **2019**, *194*, 104310. [CrossRef]

18. Briones, A.M.; Olding, R.; Sykes, J.P.; Rankin, B.A.; McDevitt, K.; Heyne, J.S. Combustion Modeling Software Development, Verification and Validation. In Proceedings of the Volume 1: Fuels, Combustion, and Material Handling, Combustion Turbines Combined Cycles, Boilers and Heat Recovery Steam Generators, Virtual Plant and Cyber-Physical Systems, Plant Development and Construction, Renewable Energy Systems, American Society of Mechanical Engineers, 24–28 June 2018; Volume 3, pp. 125–180. [CrossRef]
19. Mueller, M.E.; Raman, V. Model form uncertainty quantification in turbulent combustion simulations: Peer models. *Combust. Flame* **2018**, *187*, 137–146. [CrossRef]
20. Wang, H.; Hawkes, E.R.; Zhou, B.; Chen, J.H.; Li, Z.; Aldén, M. A comparison between direct numerical simulation and experiment of the turbulent burning velocity-related statistics in a turbulent methane-air premixed jet flame at high Karlovitz number. *Proc. Combust. Inst.* **2017**, *36*, 2045–2053. [CrossRef]
21. Hochgreb, S. Mind the gap: Turbulent combustion model validation and future needs. *Proc. Combust. Inst.* **2019**, *37*, 2091–2107. [CrossRef]
22. Driscoll, J.F. Turbulent premixed combustion: Flamelet structure and its effect on turbulent burning velocities. *Prog. Energy Combust. Sci.* **2008**, *34*, 91–134. [CrossRef]
23. Kuo, K. *Principles of Combustion*, 2nd ed.; Wiley-Interscience: Hoboken, NJ, USA, 2005.
24. Warnatz, J.; Maas, U.; Dibble, R. *Combustion*, 4th ed.; Springer: Berlin/Heidelberg, Germany; New York, NY, USA, 2005.
25. Neufeld, P.D.; Janzen, A.R.; Aziz, R.A. Empirical Equations to Calculate 16 of the Transport Collision Integrals Ω (l, s)* for the Lennard-Jones (12–6) Potential. *J. Chem. Phys.* **1972**, *57*, 1100–1102. [CrossRef]
26. Kéromnès, A.; Metcalfe, W.K.; Heufer, K.A.; Donohoe, N.; Das, A.K.; Sung, C.J.; Herzler, J.; Naumann, C.; Griebel, P.; Mathieu, O.; et al. An experimental and detailed chemical kinetic modeling study of hydrogen and syngas mixture oxidation at elevated pressures. *Combust. Flame* **2013**, *160*, 995–1011. [CrossRef]
27. Hirschfelder, J.; Curtiss, C.; Bird, R. *Molecular Theory of Gases and Liquids*, revised ed.; Wiley-Interscience: New York, NY, USA, 1964.
28. Kee, R.; Coltrin, M.; Glarborg, P. *Chemically Reacting Flow*; Wiley: New York, NY, USA, 2003.
29. Coffee, T.P.; Heimerl, J.M. Transport Algorithms for Premixed, Laminar Steady-State Flames. *Combust. Flame* **1981**, *43*, 273–289. [CrossRef]
30. Goloviznin, V.M.; Karabasov, S.A.; Kondakov, V.G. Generalization of the CABARET scheme to two-dimensional orthogonal computational grids. *Math. Model. Comput. Simul.* **2014**, *6*, 56–79. [CrossRef]
31. Ivanov, M.F.; Kiverin, A.D.; Galburt, V.A. A Computational Study of the External Shock-Wave Impact on the Combustion Regime. *Combust. Sci. Technol.* **2010**, *182*, 1683–1692. [CrossRef]
32. Baum, H.; Rehm, R. The equations of motion for thermally driven, buoyant flows. *J. Res. NBS* **1978**, *83*, 297–308.
33. Briggs, W. *A Multigrid Tutorial*; SIAM: Society for Industrial and Applied Mathematics: Philadelphia, PA, USA, 1987.
34. Zhou, G. Numerical Simulations of Physical Discontinuities in Single and Multi-Fluid Flows for Arbitrary Mach Numbers. Ph.D. Thesis, Chalmers Univ. of Tech., Goteborg, Sweden, 1995.
35. Sánchez, A.L.; Williams, F.A. Recent advances in understanding of flammability characteristics of hydrogen. *Prog. Energy Combust. Sci.* **2014**, *41*, 1–55. [CrossRef]
36. Pareja, J.; Burbano, H.J.; Ogami, Y. Measurements of the laminar burning velocity of hydrogen–air premixed flames. *Int. J. Hydrogen Energy* **2010**, *35*, 1812–1818. [CrossRef]
37. Dahoe, A. Laminar burning velocities of hydrogen–air mixtures from closed vessel gas explosions. *J. Loss Prev. Process. Ind.* **2005**, *18*, 152–166. [CrossRef]
38. Bivol, G.; Gavrikov, A.; Golub, V.; Elyanov, A.; Volodin, V. 3D surface of an unstable hydrogen–air flame. *Exp. Therm. Fluid Sci.* **2021**, *121*, 110265. [CrossRef]
39. Ivanov, M.; Kiverin, A.; Yakovenko, I.; Liberman, M. Hydrogen–oxygen flame acceleration and deflagration-to-detonation transition in three-dimensional rectangular channels with no-slip walls. *Int. J. Hydrogen Energy* **2013**, *38*, 16427–16440. [CrossRef]
40. Yanez, J.; Kuznetsov, M.; Grune, J. Flame instability of lean hydrogen–air mixtures in a smooth open-ended vertical channel. *Combust. Flame* **2015**, *162*, 2830–2839. [CrossRef]